Materials and Structures
DOI 10.1617/s11527-009-9544-5

ORIGINAL ARTICLE

Application of ECC for bridge deck link slabs

Michael D. Lepech · Victor C. Li

Received: 11 July 2007 / Accepted: 11 June 2009

Abstract In this article, the application of ECC in a bridge deck link slab is described. The unique ultra high tensile ductility and tight crack width of self-consolidating ECC is exploited in this application to improve bridge deck constructability, durability, and sustainability. Design guidelines and material specifications were developed for implementation of this ECC link slab technology. A construction project implementing these guidelines and specifications was conducted in 2005 on an ECC-concrete bridge deck in southeast Michigan, USA. This article summarizes the experience of this project.

Keywords Engineered Cementitious Composite · ECC · HPFRCC · Link slab · Jointless bridge · Sustainability

M. D. Lepech · V. C. Li (✉)
Department of Civil and Environmental Engineering, University of Michigan, 2330 G.G. Brown, Ann Arbor, MI 48109, USA
e-mail: vcli@umich.edu

M. D. Lepech
Department of Civil and Environmental Engineering, Stanford University, 285B Yang and Yamazaki Energy and Environment Building, 473 Via Ortega Street, Stanford, CA 94305-4020, USA
e-mail: mlepech@stanford.edu

Published online: 30 July 2009

1 Introduction

Large scale highway and superhighway infrastructure remains a backbone of national and international trade supporting the economies of both highly developed and developing nations worldwide. In 2002 alone, commercial freight transported on the United States interstate highway system accounted for 8.3 billion metric tons of shipments valued at over US$6.6 trillion [1]. Within the European Union, nearly half (44.2%) of all freight transport move by roadway [2]. The growing popularity of the Toyota Production System (TPS), just-in-time operation, and lean manufacturing has increased freight traffic by demanding high frequencies of smaller deliveries. Many nations however, continue to allow the condition of national infrastructure to become exceedingly poor, mainly due to a persistent lack of funding, increasing traffic volumes, and heavier loads on roadways [3]. This was exemplified by the recent catastrophic collapse of the I-35W in Minneapolis, Minnesota USA.

Many infrastructure maintenance and repair methods have been proposed and instituted, ranging from the use of high strength concrete [4] to the use of epoxy coated reinforcing steel [5] on bridge decks, each with varying degrees of success. However, none of these solutions target the inherent shortfall of concrete brittleness, which results in cracking when loaded. These cracks, with width difficult to be controlled in a reliable manner, typically allow salt

water to contact the reinforcing steel, thereby causing corrosion through steel oxidation and concrete cover spalling, and ultimately leading to structural failure. A new type of concrete material that does not crack under loading to enhance durability, provides the ductility of reinforced concrete with partial to complete elimination of corrosion-prone reinforcing steel, and remains cost competitive with current materials, would be ideal for both new and rehabilitative infrastructure projects.

Within the United States, a major source of bridge deterioration requiring constant maintenance is mechanical expansion joints installed between adjacent simple span bridge decks [6]. While these expansion joints are essential to accommodate the large thermal deformations of the adjacent steel or prestressed concrete girder decks, the tendency of these joints to quickly fall into disrepair and eventually leak is a constant source of deterioration of the entire superstructure. Water from the deck, saturated with de-icing salts during cold weather, leaks through deteriorated joints and ultimately corrodes the ends of steel girders, or penetrates into precast concrete girders and corrodes the reinforcing strands. The economic cost and backlog of expansion joint maintenance have been a continuous source of concerns to departments of transportation. Proposed solutions to this problem include the development of continuous bridge decks or integral abutment bridges which seek to eliminate mechanical expansion joints by using an uninterrupted deck surface over multiple spans. However, these solutions are only applicable to new construction and present significant design complications within the superstructure or substructure when compared to simple bridge span design.

Recent research on Engineered Cementitious Composites (ECC), a type of High Performance Fiber Reinforced Cementitious Composite (HPFRCC), has shown them to be both highly durable and well suited for large infrastructure applications [7]. The primary reason for this high performance is the ability of ECC to strain harden under uniaxial tension while forming large numbers of microcracks up to an ultimate strain capacity typically over 4% as shown in Fig. 1. This large strain capacity is over 400 times that of normal concrete. However, unlike many other cement-based composites, this high level of tensile strain is not associated with large crack width openings. Typically, cracks within ECC material open to a maximum of between 50 and 70 μm during early strain hardening stages (i.e. below 1% tensile strain) and remain at that width under additional tensile strain up to failure (Fig. 1). These unique characteristics can be attributed to deliberate micromechanical tailoring performed on the three phases within the composite; fiber, matrix, and fiber/matrix interface [8, 9]. Example ECC mix proportions for this demonstration study are shown in Table 1.

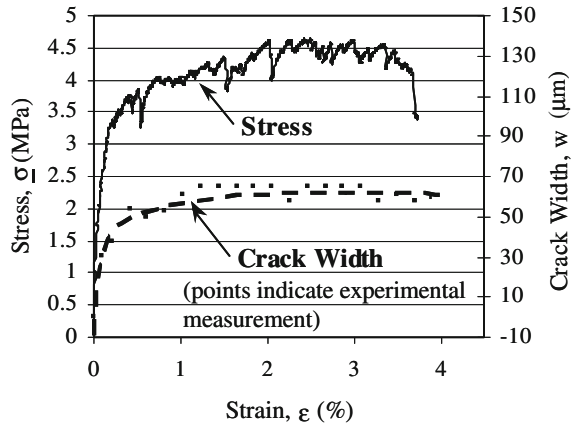

Fig. 1 ECC stress–strain response and crack width development under uniaxial tension

Table 1 Mix proportions for ECC material

Material	Proportion (by weight)
Cement	1.0
Sand	0.8
Fly ash	1.2
Water	0.59
Superplasticizer	0.015
Fiber (vol fraction)	0.02

To allow designers to maintain simple span design assumptions, and allow for retrofitting of existing bridge structures, the use of ECC "link slabs", rather than mechanical expansion joints between adjacent bridge spans, is proposed in this project. By removing the expansion joint and replacing a portion of the two adjacent decks with a section of ECC material overtop the joint, a continuous deck surface is constructed. The unique capability of ECC material to deform up to 4% strain in uniaxial tension while maintaining low crack widths allows the ECC link

slab to accommodate the deformations imposed by the adjacent decks (i.e. due to thermal expansion and contraction) while protecting the underlying superstructure and substructure from corrosives present on the deck surface.

2 Link slab design

2.1 Link slab design using conventional reinforced concrete

Typical to many regional and state departments of transportation within the US, the State of Michigan Department of Transportation (MDOT) has actively engineered and constructed solutions to the expansion joint problem. Prior to implementing ECC link slab technology, MDOT constructed a number of concrete link slabs within Michigan. These link slabs are designed according to guidelines proposed by Zia et al. [10] and Caner and Zia [11] in conjunction with the North Carolina Department of Transportation. These guidelines are based on previous research consisting of theoretical analysis and laboratory experiments of simple span bridges (both steel and prestressed concrete girders) utilizing concrete link slabs to create jointless bridge decks.

Unlike ECC material, concrete does not exhibit large tensile strain capacities and microcracking behaviors and therefore must be heavily reinforced to keep crack widths within a concrete link slab below acceptable serviceability limits allowed by the American Association of State and Highway Transportation Officials (AASHTO) bridge design code. This high reinforcement ratio within concrete link slabs unnecessarily stiffens a concrete link slab. Due to the inherently tight crack widths in ECC, a high steel reinforcement ratio for crack control is not necessary allowing the ECC link slab to act as a hinge connecting the two adjacent spans and allowing for more simple design. The lower stiffness of ECC material, especially in the microcracked state, would further enhance this benefit. Such hinging action (Fig. 2) was found successful in experimental testing by Caner and Zia [11].

Apart from the unintended stiffness increase resulting from excessive crack control reinforcement, construction of concrete link slabs was found to be highly sensitive to poor construction practices. A large majority of concrete link slabs within Michigan which have shown distress or required maintenance were found to have been designed with too little reinforcement, or the reinforcement was not installed properly by the contractor [13]. This was attributed to the unfamiliarity of design engineers with the complicated concrete link slab design procedure and construction worker's reluctance to place unconventionally dense reinforcement within concrete link slabs. Attempting to mitigate this high sensitivity to design and field construction practices, ECC link slab performance is more dependent on inherent ECC material properties, such as high strain capacity and tight crack widths, rather than on the placement of reinforcement.

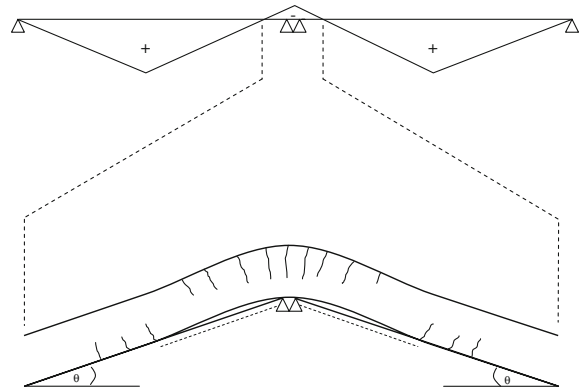

Fig. 2 Bridge moment distribution and link slab hinging mechanism [12]

2.2 Design of an ECC link slab

For use across the State of Michigan, ECC link slabs in this project were designed under the American Association of State and Highway Transportation Officials LRFD Bridge Design Manual [14]. Alterations to this design process can be made to bring ECC link slab design in line with other international infrastructure design codes as needed.

The overall length of the link slab and the length of the link slab debond zone are calculated in Eqs. 1 and 2, respectively.

$$L_{ls} = 0.075(L_1 + L_2) + G_{1-2} \quad (1)$$

$$L_{dz} = 0.05(L_1 + L_2) + G_{1-2} \quad (2)$$

where L_{ls} is the overall length of the link slab in millimeters, L_1 and L_2 are the span lengths of the two adjacent bridge spans in millimeters, $G_{1\text{-}2}$ is the

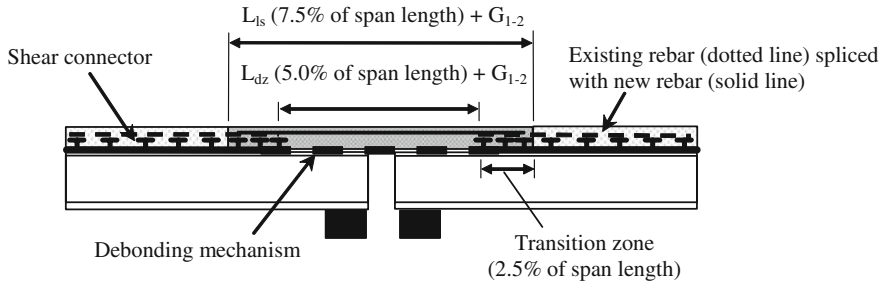

Fig. 3 Schematic of ECC link slab

length of any gap between the girders of the two adjacent spans in millimeters, and L_{dz} is the length of the link slab debond zone in millimeters.

The debond zone is the center section of the link slab in which all shear connectors between the girder and deck are removed to prevent composite action between girder and deck (Fig. 3). Along with removal of shear connectors, a mechanical debonding mechanism is secured to the top flange of the girder to further prevent shear transfer between the girder and deck. This debonding mechanism may be either standard roofing tar paper (for use with steel girders) or plastic sheeting (for use with precast concrete girders). While composite action is maintained in the adjacent spans, this debonding within the link slab allows it to function more efficiently as a hinge between the two adjacent spans while they deflect (as shown in Fig. 2). Zia et al. [10] found that up to 5% of the adjacent deck may be debonded without affecting the composite action (between deck and girder) design assumption of the adjacent spans.

Outside of the debond zone on either end of the link slab are transition zones in which shear connection and composite action between girder and deck are re-established. Due to the high shear stresses within the region, the number of shear connectors required by the design code is increased by 50%. The design of shear connectors in concrete according to the AASHTO design code has been shown conservative for shear connectors in ECC material. It is recommended to use the standard AASHTO design procedure for design of shear connectors [15].

Following the calculation of link slab length, the maximum end rotation angles of the adjacent bridge spans due to live load must be determined per the AASHTO bridge design code. This is a function of the maximum allowable deflection and the length of the adjacent spans as shown in Eq. 3.

$$\theta_{max} = \Delta_{max-short}\left(\frac{3}{L_{short}}\right) \tag{3}$$

where θ_{max} is the maximum end rotation angle of the adjacent bridge spans measured in radians, $\Delta_{max\text{-}short}$ is the maximum allowable deflection of the shorter of the two adjacent spans in millimeters, and L_{short} is the span length of the shorter of the two adjacent spans in millimeters. Since maximum allowable deflection is calculated as a function of span length (i.e. L/800), the maximum end rotation angle is often a constant for any span length. For instance, with Δ_{max} equal to L/800, θ_{max} will always be 0.00375 rad.

The uncracked moment of inertia I_{ls} is computed for the link slab per meter width of bridge deck in mm^4, as

$$I_{ls} = \frac{(1000\text{ mm})\ t_s^3}{12} \tag{4}$$

where t_s is the thickness of the bridge deck slab in millimeters.

Using the maximum end rotation of the adjacent bridge spans, and the moment of inertia of the link slab, the bending moment induced within the link slab per meter width of bridge deck due to the imposed rotations is calculated using Eq. 5.

$$M_{ls} = \frac{2E_{ECC}\ I_{ls}\ 0.001}{L_{dz}}\theta_{max} \tag{5}$$

where M_{ls} is the moment induced into the link slab per meter width of bridge deck in kN-m, E_{ECC} is the elastic modulus of ECC material in GPa, I_{ls} is the uncracked moment of inertia of the link slab in mm^4 (Eq. 4), L_{dz} is the length of the link slab debond zone in millimeters (Eq. 2), and θ_{max} is the maximum end rotation angle of the adjacent spans in radians (Eq. 3). The elastic modulus of ECC material is typically assumed as 20 GPa.

The moment induced in the link slab by the rotation of adjacent bridge spans, M_{ls}, can be viewed as the "moment demand" placed on the ECC link slab. Therefore, the uncracked moment of inertia of the link slab, I_{ls}, is used in Eq. 5. While the ECC link slab is designed and intended to function in the microcracked state (with lower moment of inertia), this higher calculation of moment demand introduces additional conservatism and safety into the ECC link slab design. This also compensates for the slight increase in sectional stiffness which would be calculated if the stiffness contribution from steel reinforcement was included. Further calculations show that ignoring this contribution of steel reinforcements to M_{ls} leads to negligible error.

Viewing M_{ls} as the imposed "moment demand", the amount of steel reinforcement within the ECC link slab must be calculated to resist this moment. The amount of steel reinforcement within the link slab is based entirely on structural load capacity and not on any crack width serviceability requirements since large tensile cracks do not form in ECC under normal load conditions [16]. To calculate the moment capacity of the ECC link slab section, a non-linear sectional analysis is used based on the assumption that ECC material remains perfectly elastic-plastic in service. While ECC material typically does show some strain hardening characteristics after first cracking as shown in Fig. 1, this strength gain will not be relied upon to once again promote conservative design practice.

The "yield strain" of the ECC material designed for this project and designated M45 is set at 0.02%. From a pool of 40 separate tensile test results, this value is chosen as a statistically representative value for the first cracking strain of ECC material and is used for the ECC link slab design. The "yield stress" of the ECC material is set at 3.45 MPa. While the actual ultimate strength is typically above this value, 3.45 MPa was again chosen as a statistically representative value from the pool of tensile test results. Statistical variation of these values has been discussed by the authors elsewhere (Fig. 4) [17].

As proposed by Caner and Zia [11], a conservative working stress of 40% of the yield strength, f_y, of the steel reinforcement is used for design. Unlike the design assumptions for concrete, in which no tensile force is carried by the concrete, a substantial stress of

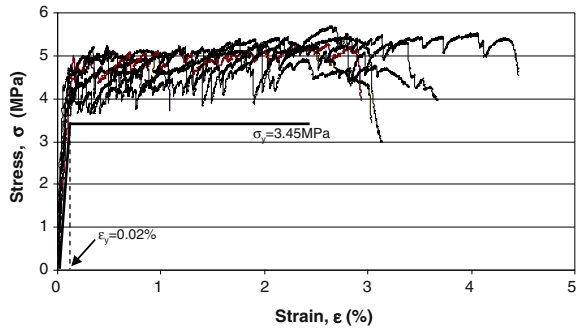

Fig. 4 ECC M45 tensile stress–strain and idealized elastic-perfectly plastic behavior

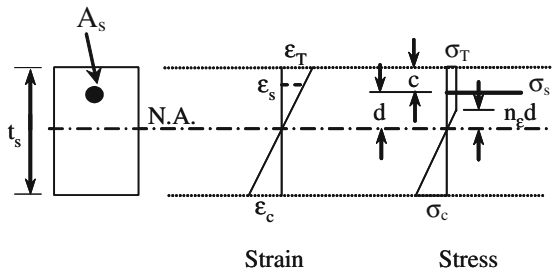

Fig. 5 Stress and strain distributions in the ECC link slab cross section carrying a negative moment

3.45 MPa is assumed to be carried by the ECC up to failure between 2 and 3% strain. Using non-linear analysis and the assumption of a linear strain distribution within the section, shown in Fig. 5, the moment capacity of the section can be computed for any steel reinforcing ratio. The reinforcement ratio is then adjusted accordingly to resist the moment due to maximum end rotation computed earlier in Eq. 5. Figure 5 also shows the cross sectional stress distribution of a reinforced ECC link slab (R/ECC).

To compute the moment capacity of the ECC link slab section, the location of the neutral axis of the section is determined through force equilibrium. However, prior to performing force equilibrium, the location of the stress "kink" in the tension region of the section, due to the elastic-plastic tensile response of ECC material, is calculated. As a result of the linear strain assumption within the section, this is done using geometry and the ratio of yield strains of steel and ECC, along with the assumption of 40% working stress in the reinforcing steel. This is shown in Eq. 6.

$$n_{\varepsilon} = \frac{\varepsilon_{y-ECC}}{0.4\varepsilon_{y-steel}} \quad (6)$$

where n_{ε} is the yield strain ratio, $\varepsilon_{y\text{-}ECC}$ is the "yield strain" of the elastic-plastic ECC behavior (0.02% as shown in Fig. 4), and $\varepsilon_{y\text{-}steel}$ is the yield strain of the reinforcing steel.

Equilibrium balance of the section is enforced to determine the location of the neutral axis. A preliminary reinforcement ratio is then selected for iterative design. The moment capacity of the ECC link slab based on this reinforcement ratio is determined and this capacity is compared to the moment induced (i.e. demanded) in the slab the beam end rotation (from Eq. 5). If moment capacity for the selected reinforcement ratio is below the moment induced, a higher reinforcement ratio is chosen and a second design iteration is performed.

Equations 7a–d are used to calculate the force within the reinforcing steel, tensile portion of ECC material, and compressive portion of ECC material per meter width of bridge deck. Equilibrium balance is completed by solving a simple non-linear equation, shown in Eq. 7e. The goal of this calculation is the determination of the value for "d".

$$T_{steel} = (0.4f_{y-steel})\rho t_s \quad (7a)$$

$$T_{ECC-1} = f'_t((1\text{-}n_{\varepsilon})d + c) \quad (7b)$$

$$T_{ECC-2} = 0.5f'_t n_{\varepsilon} d \quad (7c)$$

$$C_{ECC} = 0.5f'_t\left(\frac{1}{n_{\varepsilon}d}\right)(t_s - d - c)^2 \quad (7d)$$

$$T_{steel} + T_{ECC} + C_{ECC} = 0 \quad (7e)$$

where T_{steel} is the tension force in the reinforcing steel per meter width of bridge deck in kN, $f_{y\text{-}steel}$ is the yield strength of the steel in MPa, ρ is the steel reinforcement ratio, t_s is the deck slab thickness in millimeters, $T_{ECC\text{-}1}$ and $T_{ECC\text{-}2}$ are tension forces in the ECC per meter width of bridge deck in kN, f'_t is the assumed tensile strength of the ECC material in MPa, n_{ε} is the yield strain ratio computed using Eq. 6, d is the distance from the neutral axis to the centroid of reinforcing steel in millimeters, c is the distance from the tensile face of the slab to the centroid of the reinforcing steel in millimeters, C_{ECC} is the compressive force in the ECC slab per meter width of bridge deck in kN. Dimensions are shown graphically in Fig. 5.

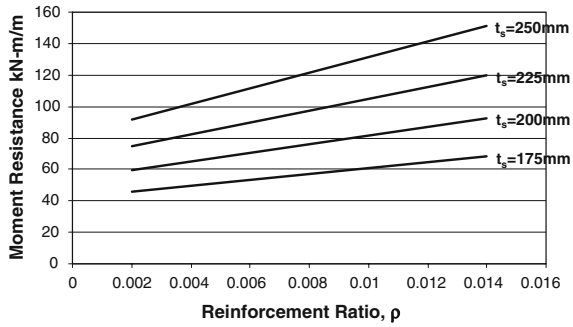

Fig. 6 ECC link slab required reinforcement ratio design chart

Using the force in each portion of the section along with the location of the neutral axis, the moment resisting contribution of each portion is used to compute the overall moment capacity of the link slab, shown in Eq. 8.

$$M_{r\text{-}ls} = \left\{ T_{steel}d + T_{ECC-1}\left(\frac{(1-n_{\varepsilon})d + c}{2} + n_{\varepsilon}d\right) + T_{ECC-2}\left(\frac{2}{3}\right)n_{\varepsilon}d + C_{ECC}\left(\frac{2}{3}\right)(t_s - d - c)\right\}\left(\frac{1}{1000}\right) \quad (8)$$

where $M_{r\text{-}ls}$ is the resisting moment capacity provided by the link slab per meter width of bridge deck in kN-m.

The moment resistance, $M_{r\text{-}ls}$, calculated from Eq. 8, is compared to the moment demand induced by the imposed end rotations, M_{ls}, from Eq. 5. Starting with an assumed value for ρ, if the resistance so determined is greater than the demand, the strength design is completed using the selected reinforcement ratio. Otherwise, a higher reinforcement ratio is selected and the process iterated. Since this process can involve a number of iterations when determining the reinforcement ratio, a simple design chart has been adapted from that given previously by Li et al. [18] for several slab thicknesses t_s. This chart is shown as Fig. 6 with accompanying assumptions in Table 2. Once the moment demand is determined (Eq. 5), the reinforcement ratio required can be read off from Fig. 6 for a given slab thickness.

Finally, a specific reinforcing steel bar is selected and the required bar spacing is calculated using Eq. 9.

Table 2 ECC link slab reinforcement ratio design chart assumptions

Assumption	Value
Working stress factor [10]	40%
ECC tensile yield strain [17]	0.02%
Steel tensile yield strain	0.08%
Steel tensile yield strength	410 MPa
ECC tensile yield strength	3.45 MPa
Distance from tensile face to steel centroid, c	75 mm

$$S = \frac{A_{bar}}{\rho t_s} \tag{9}$$

where s is the spacing between the bars in millimeters, A_{bar} is the cross sectional area of the selected reinforcing steel bar size in mm^2, ρ is the finalized reinforcement ratio, and t_s is the deck slab thickness.

2.3 ECC material design checks and construction sequencing

To avoid failure of the link slab, the strain demand upon ECC material both in tension and compression must be checked to ensure it does not exceed the material capacity. Once the location of the neutral axis is found, the strain at both the compression and tension face due to live loads on the adjacent spans can be computed assuming the linear strain distribution. The strain in tension is computed using Eqs. 10a and 10b, while the compressive strain is computed using Eq. 11. If these values computed in Eqs. 10b or 11 exceed the tensile or compressive strain capacities of ECC material in laboratory testing, a new version of ECC must be designed to meet these demands. Otherwise, the length of the link slab debond zone can be lengthened to reduce the tensile demand (provided the 5% maximum is not exceeded).

$$\varepsilon_{LL} = \frac{0.4\varepsilon_{y-steel}(d + c)}{d} \tag{10a}$$

$$\varepsilon_T = \frac{\alpha_T \, \Delta T \, \beta L_{long}}{L_{dz}} + \varepsilon_{sh} + \varepsilon_{LL} \tag{10b}$$

$$\varepsilon_C = \frac{0.4\varepsilon_{y-steel}(t_s - d - c)}{d} \tag{11}$$

where ε_{LL} is the tensile strain due to live load moment, $\varepsilon_{y\text{-}steel}$ is the yield strain of the reinforcing steel, d is the distance from the neutral axis to the centroid of reinforcing steel in mm, c is the distance from the tensile face of the slab to the centroid of the reinforcing steel in mm, ε_T is the maximum total tensile strain in the ECC link slab due to live load moment, shrinkage strains, and temperature deformations of adjacent spans, α_T is the coefficient of thermal expansion for girder material in 1/°C, Δ_T is the seasonal temperature range in °C, β is a design value taken as 2.0 for joints with two roller bearings and 1.0 for all other joints, L_{long} is the span length of the longer adjacent span in millimeters, L_{dz} is the length of the link slab debond zone in millimeters, ε_{sh} is the shrinkage strain of ECC taken as 0.001 [19], and ε_c is the maximum compressive strain in the link slab.

The designer must perform a number of other checks. It should be verified that existing abutments can withstand additional thermal movement if all existing expansion joints are removed. If this is not the case, the existing backwall must be replaced with a sliding backwall. The designer should also verify that the existing pier columns can withstand additional thermal movement if all existing expansion joints are removed. The existing bearings should be checked to verify they can accommodate additional thermal movements.

Inherently assumed in this design example is a deck pour schedule which places the ECC link slab last, since the maximum end rotation of the link slab is calculated using only the maximum allowable deflection under live load ($\Delta_{max} = L/800$). If the link slab is cast before all dead loads are applied to the adjacent spans, the combined dead load end rotation and live load end rotation may exceed the value calculated in Eq. 3. To this end, care must be taken during construction to place all dead loads on adjacent spans prior to ECC link slab casting.

3 Experimental validation and demonstration project

3.1 Link slab experimental testing

Large scale laboratory testing of ECC link slabs was conducted by Kim et al. [12] to investigate the load capacity and fatigue performance of ECC link slabs, along with the development of cracking on the tensile face of the ECC link slab. Kim found that ECC

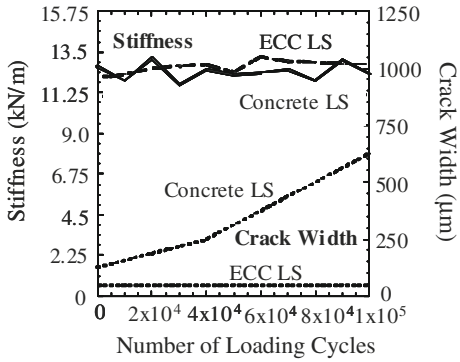

Fig. 7 Link slab stiffness and crack width development under cycle loads [12]

material was a suitable choice for construction of link slabs to replace conventional mechanical expansion joints. The large tensile strain capacity, facilitated by saturated multiple cracking with widths of 60 μm meet all structural and durability needs of a link slab application. During monotonic loading, a lower stress in the reinforcement was seen in ECC link slabs than in concrete link slabs, allowing for further reduction of reinforcement levels. Cyclic tests using a full depth (225 mm) link-slab and steel girder assembly covering the length represented in Fig. 2 revealed that both ECC and concrete link slabs show no degradation of stiffness after 100,000 loading cycles (Fig. 7) with rotational amplitude equal to 0.00375 rad. However, crack widths in the concrete link slab grew to over 600 μm during cyclic testing while crack widths in the ECC link slab remained small, in all cases less than 60 μm (Fig. 7). Additionally, wheel abrasion studies were carried out on ECC slabs and were found to more than meet the minimum standards required by the State of Michigan [18].

3.2 Demonstration project

A demonstration project, in cooperation with the Michigan Department of Transportation, was completed during summer 2005. The 225 mm thick ECC link measured 5.5 m × 20.25 m. Construction included 25.5 m^3 of ECC, delivered on-site by standard ready-mix concrete trucks from a nearby batching plant. The mix design and processing requirements for large scale batching, and mixing of ECC material in ready-mix trucks are discussed in Lepech and Li [17].

Construction of the demonstration bridge took place in two phases to allow for continued use of the bridge during construction. Approximately 15 m^3 of ECC material were prepared for each half of construction (30 m^3 total for the bridge), mixed in three trucks each containing 5 m^3 of ECC. As quality

Fig. 8 **a** Location of ECC link slab, **b** placement of reinforcing steel within link slab segment, **c** placement of ECC material, **d** finishing of riding surface

Table 3 Average fresh properties of ECC link slab material

Test	Plant	Site	Required	No. of trucks
Temperature (°C)	–	26.8	–	6
Flowability diameter (cm)	61	63	76	6
Air content (%)	–	5.1	–	6

control, measurements of mix flowability, air content, and temperature were conducted for ECC samples from each truck arriving on site, along with preparing specimens for testing hardened mechanical properties. Placement of ECC material is shown in Fig. 8. Fresh and hardened properties of the ECC material are given in Tables 3 and 4, respectively. Fresh properties were determined as outlined for self-consolidating by Michigan Department of Transportation Special Provision for ECC Bridge Deck Link Slab [20] and Kong et al. [21]. Compressive strength was determined using ACTM C39. Tensile strength as strain measurements were determined as outline by Li et al. [8].

Shown in Fig. 8b, the steel reinforcement ratio used on this bridge greatly exceeds the amount determined using Eq. 8. As mentioned previously, this bridge project was designed in accordance with AASHTO load resistance factor design (LRFD) standards [14]. Within this design code, the unique tensile and cracking properties of ECC can not yet be included in the bridge design. Therefore, the link slab was over-designed assuming no tensile load capacity and crack controlling behavior. The steel reinforcement ratio nearly tripled due to this conservatism.

All minimum values set by MDOT were met, aside from the required flowability diameters. These requirements were partially relaxed following field observations which showed acceptable material homogeneity and rheological properties without a spread diameter of 76 cm. Additionally, the stiffer ECC mixture gave the general contractor confidence that the material would not flow off of the bridge due to the 2% deck crown. While there were large differences in the fresh appearance of the ECC on site (i.e. flowability), differences among the three trucks measured in the mechanical testing are relatively small. Mechanical property test results are indistinguishable between the first, second, or third truck loads.

3.3 Proof load testing

To validate the performance of the ECC link slab, static load testing was carried out immediately following construction. This allowed for validation of design assumptions and monitoring of ECC link slab response under static loading. One design assumption to be validated was that the introduction of the link slab element did not alter the fundamental assumption of simple support adopted in the original design of the adjacent composite bridge spans. Another assumption that needed validation was the magnitude of the induced strain on the negative moment carrying link slab due to live load on the bridge span.

Hence, the instrumentation adopted focused upon two response parameters of the link slab under static load—beam end rotation and maximum strain on link slab surface. The rotations of the steel girders immediately below the link slab were obtained from relative displacement measurements (at a sampling rate of 100 Hz) from LVDTs mounted on the top and bottom of abutting steel girder ends directly below the ECC link slab. The direct link slab surface tensile

Table 4 Hardened properties of ECC link slab material

Age (days)	Test								
	Compressive			Tensile strength			Tensile strain		
	Actual (MPa)	Required (MPa)	No. of tests	Actual (MPa)	Required (MPa)	No. of tests	Actual (%)	Required (%)	No. of tests
4	32.0 ± 2.0	–	12	3.4 ± 0.25	–	12	2.7 ± 0.4	–	12
7	43.9 ± 2.4	22	12	3.9 ± 0.30	3.45	12	2.5 ± 0.2	2.0	12
14	49.0 ± 2.7	27.5	12	4.2 ± 0.27	3.45	12	2.4 ± 0.3	2.0	12
28	52.4 ± 4.4	31	12	4.4 ± 0.23	3.45	12	2.2 ± 0.1	2.0	12

Table 5 Comparison of measured girder end rotations (LVDT) and analytical girder end rotations (FEM)

	Load Case 1	Load Case 2
Girder rotation (measured) (rad)	0.00076	0.00071902
Girder rotation (FEM) (rad)	0.00054	0.00091000
% Error	28.9	26.6

strain measurements were obtained from strain transducers at a sampling rate of 50 Hz, mounted directly on the deck surface. Two 6-axle HS 25-44 equivalent trucks served as static proof load. Prior to load testing, trucks were accurately weighed using a high-precision highway load station operated by the Michigan State Police. Proof load testing was conducted 8 days following ECC link slab placement.

The measured beam end rotations were found to be reasonably comparable to those derived analytically from an approximate bridge deck finite element model that assumed simply supported condition for the bridge spans. These comparisons are shown in Table 5 for two test cases—(1) with one HS 25-44 equivalent truck being placed at the maximum moment position on each of the two spans adjacent to the ECC link slab (Load Case 1), and (2) with two HS 25-44 equivalent trucks being placed at the maximum moment position of one of the spans adjacent to the ECC link slab (Load Case 2). Recognizing the many assumptions built into the analytic FEM model, the reasonable alignment of load tests results with FEM modeling results suggests that the ECC link slab performs as assumed and can function without violating the simple span assumptions inherent in the design of the existing adjacent spans.

As seen in Table 5, in Load Case 1 measured girder end rotations are greater than the predicted girder end rotations from FEM analysis while in Load Case 2 measured girder end rotations are lower than the predicted girder end rotations from FEM analysis. This may be the combination of a number of phenomena. Measured girder rotations in Load Case 2 may be lower than maximum due to the physical limitations of placing two large trucks on a small, highly skewed bridge deck. The low prediction of girder rotation may also result from lower material stiffness in the ECC link slab material. FEM model inputs were based on a large database of laboratory test data rather than the small dataset of sub-optimal field material properties determined in this demonstration project. The use of a higher elastic modulus would underestimate girder rotation and result in the relatively small girder rotation predictions shown in Table 5.

The directly measured link slab top surface strains from strain transducers (0.004 and 0.0025% for the two load cases) correlated well with those calculated from measured beam end rotations, consistent with the assumption of pure bending of the ECC link slab uncoupled from the girder, as intended in the link slab design (Fig. 2). Without the effective performance of the debond zone, the link slab would have formed a kink on top of the girder end gap and the tensile strain on the top surface of the ECC link slab would have been unacceptably large. As the measurements from the strain transducers and beam end rotations confirm, these strains are significantly below the tensile strain capacity (specified as a minimum of 2% in design documents, and with actual values given in Table 4) of the ECC material, designed to absorb the much higher strain expected to be induced by temperature variation (girder expansion and contraction).

4 Conclusion

Within this demonstration project, a new cementitious composite was used on a bridge deck within Michigan to replace a conventional joint within the deck. The composite used, called Engineered Cementitious Composites or ECC, shows a unique behavior of pseudo-strain hardening under tensile loads. The design concepts behind this work have been detailed herein.

Following the authoring of design and construction documents, preliminary steps leading toward large-scale trial mixing of ECC were undertaken. These large-scale trial mixes confirmed that large scale mixing of ECC material was possible and could result in a material that maintained its high performance in large quantity processing with conventional ready-mix equipment. In accordance with the bridge contractor's schedule, the link slab was cast over the fall of 2005 requiring 30 m^3 of ECC material. Quality control of the material sampled from the ready-mix delivery trucks was conducted for both compressive and tensile response, and determined to be in accordance with the ECC construction contract.

Finally, a full scale load test was conducted to explore the structural response of the constructed ECC link slab. These load tests validated that the incorporation of an ECC link slab in placement of a conventional expansion joint did not alter the simply supported nature of the bridge spans, and that ample strain capacity of the ECC is reserved for temperature induced straining as designed.

Two years after this ECC link slab was placed, the performance of this link slab remains unchanged. With further long term performance monitoring and additional demonstration experience, ECC link slab can be an effective replacement of conventional expansion joints resulting in significantly reduced bridge deck maintenance needs.

Acknowledgements The authors would like to graciously thank the Michigan DOT and the US National Science Foundation MUSES Grant (CMS-0223971 and CMS-0329416) for partially funding this research, in particular Mr. Roger Till, P.E. and Mr. David Juntunen, P.E. of MDOT. The authors would also like to thank Professor Jerome P. Lynch and Mr. Tsung-Chin Hou for the administration of proof load testing, and Dr. Gregor Fischer and Dr. Yun Yong Kim for their advice and discussions.

References

1. USDOT–FHWA (2003) Highway statistics 2002. Washington, DC, USA
2. Directorate-General for Energy and Transport (2006) The annual energy and transport review for 2004. European Communities, Belgium
3. American Society of Civil Engineers (ASCE) (2007) 2005 report card for America's infrastructure. http://www.asce.org/reportcard/2005/index.cfm. Accessed 28 Oct 2007
4. Hokoku K (2001) High strength concrete technology. J Taiheiyo Cem Corp 140:47–59
5. Al-Zahrani MM, Al-Dulaijan SU, Ibrahim M, Saricimen H, Sharif FM (2002) Effect of waterproofing coatings on steel reinforcement corrosion and physical properties of concrete. Cem Concr Compos 24(1):127–137
6. Michigan Department of Transportation (MDOT) (2003) Bridge preservation timeline. Construction & Technology Division, Michigan Department of Transportation, Lansing
7. Li VC (2003) On engineered cementitious composites (ECC)—a review of the material and its applications. J Adv Concr Technol 1(3):215–230
8. Li VC, Wu C, Wang S, Ogawa A, Saito T (2002) Interface tailoring for strain-hardening PVA-ECC. ACI Mater J 99(5):463–472
9. Yang EH, Li VC (2007) Strain-hardening fiber cement optimization and component tailoring by means of a micromechanical model. J Constr Build Mater (accepted)
10. Zia P, Caner A, El-Safte AK (1995) Jointless bridge decks. Research project 23241-94-4. Center for Transportation Engineering Studies, North Carolina State, pp 1–117
11. Caner A, Zia P (1998) Behavior and design of link slabs for jointless bridge decks. PCI J 43:68–80
12. Kim YY, Fischer G, Li VC (2004) Performance of bridge deck link slabs designed with ductile ECC. ACI Struct J 101(6):792–801
13. Gilani A, Jansson P (2004) Link slabs for simply supported bridges—Michigan Department of Transportation report no. MDOT SPR-54181. Michigan DOT, Lansing
14. American Association of State Highway and Transportation Officials (AASHTO) (2004) AASHTO LFRD bridge design specifications, 3rd edn. AASHTO, Washington
15. Li VC, Fischer G, Kim Y, Lepech M, Qian S, Weimann M, Wang S (2003) Durable link slabs for jointless bridge decks based on strain-hardening cementitious composites. Michigan Department of Transportation report no. RC-1438, pp 1–96
16. Lepech MD, Li VC (2006) Long term durability performance of engineered cementitious composites. J Restor Build Monum 12(2):119–132
17. Lepech MD, Li VC (2008) Large scale processing of engineered cementitious composites. ACI Mater J 105(4): 358–366
18. Li VC, Lepech M, Li M (2005) Field demonstration of durable link slabs for jointless bridge decks based on strain-hardening cementitious composites. Michigan Department of Transportation report no. RC-1471, pp 1–147
19. Weimann MB, Li VC (2003) Hygral behavior of engineered cementitious composites (ECC). Int J Restor Build Monum 9(5):513–534
20. Michigan Department of Transportation (2005) Special provision for ECC bridge deck link slab. Construction and Technology Division, Lansing
21. Kong HJ, Bike S, Li VC (2003) Development of a self-consolidating engineered cementitious composite employing electrosteric dispersion/stabilization. Cem Concr Compos 25(3):301–309